



Low-Temperature Adaptation Targets Genome Packing Reactions in an Icosahedral Single-Stranded DNA Virus

Elizabeth T. Ogunbunmi, a,b Samuel D. Love, a Katherine A. Rhodes, a,c Adriana Morales, d Margaret H. Wilch, b Jeremy Jonas, d Dentley A. Fane

- ^aThe BIO5 Institute, University of Arizona, Tucson, Arizona, USA
- ^bDepartment of Molecular and Cellular Biology, University of Arizona, Tucson, Arizona, USA
- ^cDepartment of Immunobiology, University of Arizona, Tucson, Arizona, USA
- dTucson High Magnet School, Tucson, Arizona, USA

ABSTRACT ØX174, G4, and α 3 represent the three sister genera of a *Microviridae* subfamily. α 3-like genomes are considerably larger than their sister genera genomes, yet they are packaged into capsids of similar internal volumes. They also contain multiple A* genes, which are nested within the larger A gene reading frame. Although unessential under most conditions, A* proteins mediate the fidelity of packaging reactions. Larger genomes and multiple A* genes may indicate that genome packaging is more problematic for α 3-like viruses, especially at lower temperatures, where DNA persistence lengths would be longer. Unlike members of the other genera, which reliably form plaques at 20°C, α 3-like phages are naturally cold sensitive below 28°C. To determine whether there was a connection between the uniquely α 3-like genome characteristics and the cold-sensitive phenotype, the α 3 assembly pathway was characterized at low temperature. Although virions were not detected, particles consistent with off-pathway packaging complexes were observed. In a complementary evolutionary approach, α 3 was experimentally evolved to grow at progressively lower temperatures. The two major responses to cold adaptation were genome reduction and elevated A* gene expression.

IMPORTANCE The production of enzymes, transcription factors, and viral receptors directly influences the niches viruses can inhabit. Some prokaryotic hosts can thrive in widely differing environments; thus, physical parameters, such as temperature, should also be considered. These variables may directly alter host physiology, preventing viral replication. Alternatively, they could negatively inhibit infection processes in a host-independent manner. The members of three sister *Microviridae* genera (canonical species ØX174, G4 and α 3) infect the same host, but α 3-like viruses are naturally cold sensitive, which could effectively exclude them from low-temperature environments (<28°C). Exclusion appeared to be independent of host cell physiology. Instead, it could be largely attributed to low-temperature packaging defects. The results presented here demonstrate how physical parameters, such as temperature, can directly influence viral diversification and niche determination in a host-independent manner.

KEYWORDS DNA packaging, *Microviridae*, bacteriophage evolution, experimental evolution, single-stranded DNA

The canonical species \emptyset X174, G4, and α 3 represent three sister genera of a microvirus subfamily (1). Although gene size and order are conserved between the genera, α 3-like genomes have three distinguishing characteristics. First, the size of the intercistronic region between genes H and A (Fig. 1) is approximately 700 nucleotides longer. In addition to a conserved transcription terminator and promoter (2–6), it contains five additional open reading frames (ORFs) (1), which appear to have undergone purifying selection

Editor Colin R. Parrish, Cornell University

Copyright © 2022 American Society for
Microbiology. All Rights Reserved.

Address correspondence to Bentley A. Fane, bfane@email.arizona.edu.

The authors declare no conflict of interest.

Received 11 December 2021 Accepted 10 February 2022 Published 14 March 2022

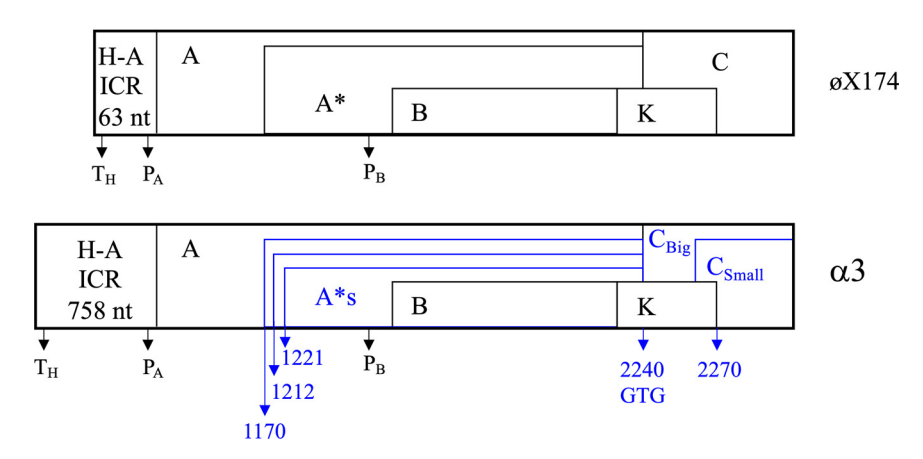


FIG 1 Genetic maps of the \emptyset X174 and α 3 genomes (not drawn to scale) from the start of the H-A intercistronic region (H-A ICR) to the end of gene C. Promoters and terminators are, respectively, depicted by the letters P and T. There are likely three A* genes in α 3. The two starting at nucleotides 1212 and 1221 have been previously recognized. The one starting at nucleotide 1170 was identified in this study.

(1). While lab-adapted strains have acquired single-base frameshifts within some of these reading frames, the region's length has been maintained within the genera. Gene products have yet to be associated with these ORFs. Second, α 3-like genomes encode two C proteins, C_S and C_B (7). During DNA replication (Fig. 2) protein C regulates the switch from double-stranded (ds) to single-stranded (ss) DNA synthesis (8). The smaller version, C_S , is translated from an internal start codon within the C_B reading frame. Only one version, either C_B or C_S , is required for replication. Third, α 3-like viruses have multiple A* genes, whereas the viruses in the other genera have only one (1). A* proteins are N-terminal truncated versions of larger A proteins (4, 9), which mediate rolling circle replication (10). Although the ØX174 protein A* is unessential for viability, elevating A* protein levels or duplicating the protein's DNA target site rescues lethal packaging defects (11). Comparable A/A*-like arrangements are widespread in ssDNA viruses that simultaneously synthesize and package DNA (12, 13).

In addition to the above-described genotypic distinctions, the α 3-like viruses exhibit a dramatic phenotypic difference. ØX174-like and G4-like phages form plaques at temperatures as low as 20°C, whereas α 3-like viruses are exquisitely cold sensitive. Plaque formation ceases below 28°C (1, 14). In general, genome packaging will be more difficult at lower temperatures due to increased DNA persistence lengths (15). This may be particularly problematic for the α 3-like viruses, which must package larger genomes into capsids volumetrically comparable to ØX174 and G4 (16–18). This might partially explain the evolution of multiple A*genes within the α 3 genera. To determine whether there is a relationship between cold-sensitivity and DNA packaging, low-temperature α 3 assembly and packaging were characterized; a classical genetic analysis, with a twist, was performed, and α 3 was experimentally evolved at successively lower temperatures.

RESULTS

 α 3 DNA packaging restricts replication below 28°C. As previously documented (1, 14), α 3 plaque formation is cold sensitive (Fig. 3, blue bars no. 1 and no. 4). At 28°C, plating efficiency was approximately an order of magnitude lower than that of the 37°C positive control, but it was highly variable. Plaques were extremely small and faint, which hindered accurate counts. At 26°C, a more restrictive condition, plating efficiency fell 6 orders of magnitude.

To determine the infection products generated at 26°C, 28°C, and 37°C, concentrated 1.0-mL extracts were prepared from 1 \times 10¹⁰ infected cells (see Materials and Methods). The titer of the 37°C extract was 7.0 \times 10¹¹ PFU/ml, indicating a productive infection. In contrast, the respective titers of the 28°C and 26°C extracts were 6.0 \times 10⁹

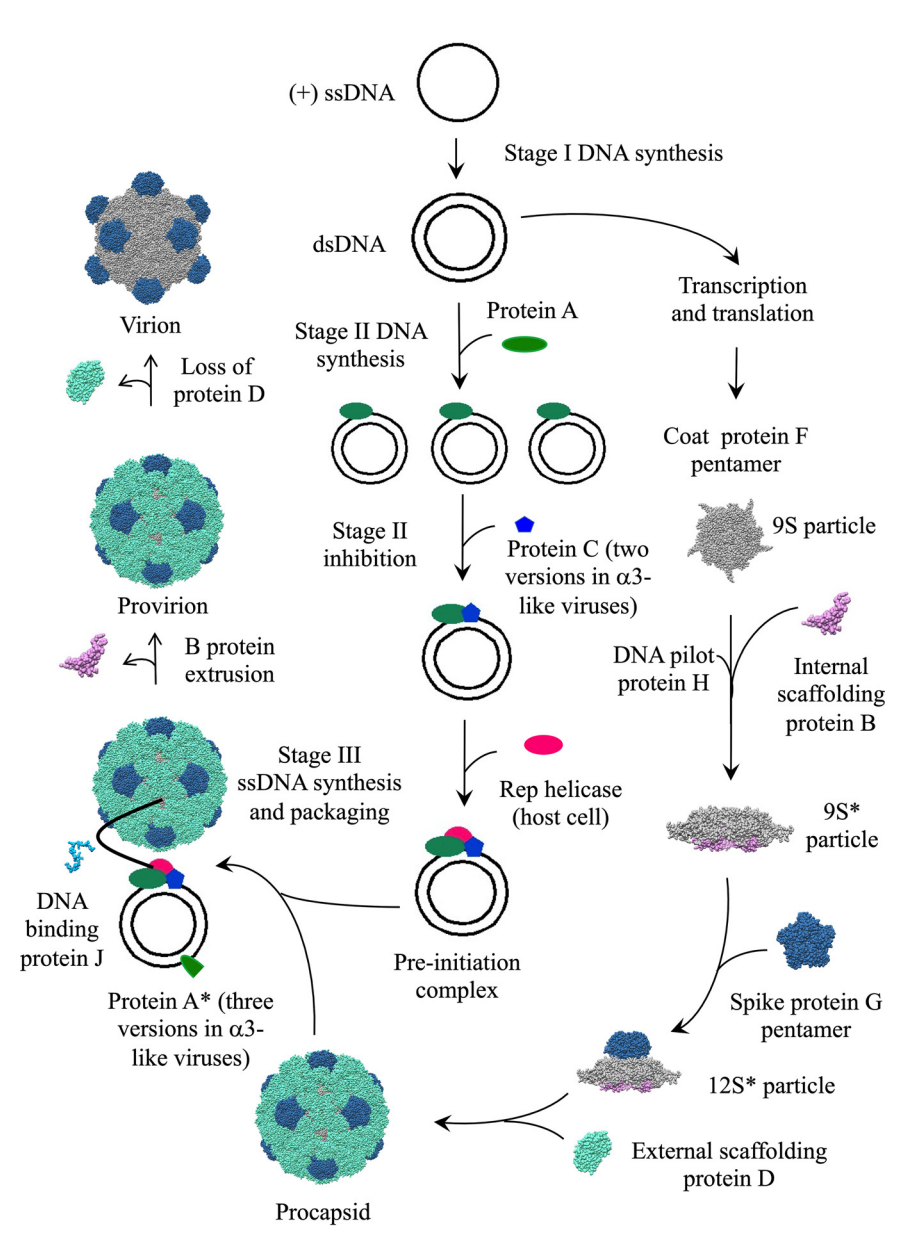


FIG 2 Generalized life cycle of the ØX174-, G4-, and α 3-like viruses. All illustrated proteins, apart from the rep helicase are encoded by the viral genome. DNA replication requires an additional 13 host cell proteins. Viral protein A mediates rolling circle DNA replication (stage II DNA synthesis), whereas viral protein C inhibits this process. The 9S, 9S*, and 12S* particles are intermediates in procapsid morphogenesis, which is mediated by two scaffolding proteins, an internal and external species, proteins B and D, respectively.

and 5.0×10^8 PFU/mL. Extracts were layered atop a 5 to 30% sucrose gradient to separate infection products. After centrifugation, the gradients were divided into approximately 40 fractions. To generate sedimentation profiles (Fig. 3), the biological material in each fraction was quantified by UV spectroscopy.

The sedimentation profile obtained from the 37°C extract (Fig. 3, magenta) displayed the typical pattern seen in øX174 experiments; two distinct peaks formed from faster and slower migrating populations. The material in the faster migrating peak contained virions. It was considerably more infectious (6.0×10^{11} PFU/mL) than the material in the slow migrating peak (5.0×10^{8} PFU/mL). In contrast, virion peaks were not evident in the 28°C (lavender) and 26°C (blue) profiles; however, low levels of phage were detected in plaque assays (Fig. 3). Slow migrating material was also evident in

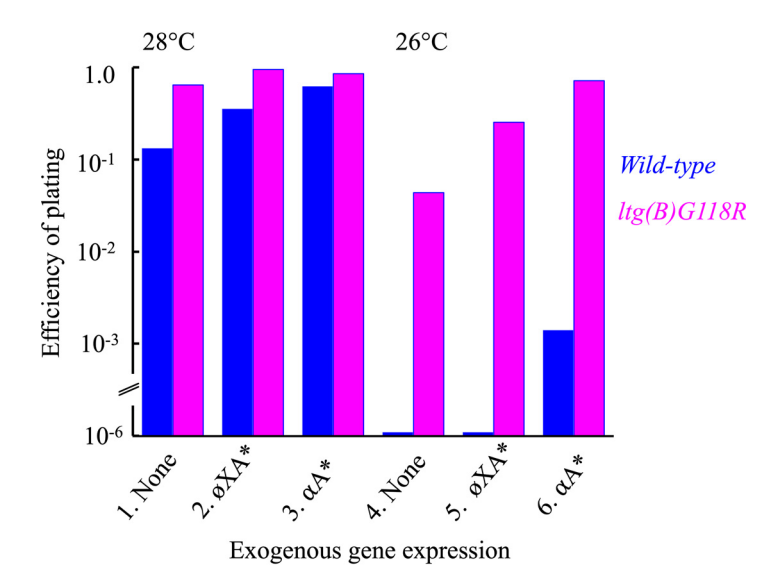


FIG 3 Low-temperature plating efficiency of wild-type $\alpha 3$ and ltg(B)G118R. Wild-type plating efficiency is depicted in blue, whereas ltg(B)G118R plating efficiency is depicted in magenta. This mutant was isolated on cells expressing a cloned A* gene at 26°C. Values were normalized to titers obtained at 37°C. Numbers 1 to 6 indicate whether cells were expressing a cloned øX174 or $\alpha 3$ A* genes. Plating efficiencies within the 10^{-1} to 10^{-3} range are somewhat approximated. Plaques displayed a faint pin-prick morphology, which hindered accurate counts.

the 28°C sedimentation profile, as a distinct plateau, whereas the 26°C profile contained a gradual slope. In øX174 experiments, the slow migrating peak typically contains unfilled, degraded procapsids that have lost external scaffolding proteins (17, 19–22). However, further characterization of the slow α 3 particles indicated key differences (see below).

To correlate the distribution of the viral coat protein within the gradient to the sedimentation profiles, gradient fractions were examined by SDS-PAGE (Fig. 4A). For the 37°C fractions, coat protein concentrations increased in fractions corresponding to the virion and slow migrating peaks. In addition, coat protein concentrations were high in the topmost fractions, which would contain the smaller early assembly intermediates and unassembled coat protein monomers. Similar correlations were observed between coat protein concentrations and the other sedimentation profiles. For the 28°C gradients, the coat protein was more prevalent in the fractions corresponding to the plateau than the virion region. It decreases after the plateau before becoming more intense at the top of the gradient. Coat protein concentrations steadily increase in the 26°C fractions, which may indicate a heterogenous mix of partially assembled or degraded products. Side by side comparisons of key gradient fractions are depicted in Fig. 5B, in which the other structural proteins are visible in some samples. Regardless of the infection temperature, the viral proteins are most prevalent in the uppermost fractions, indicating that α 3 can produce its proteins at lower temperatures, and by extension, it indicates that the (-) DNA strand, which serves as the transcription template, was synthesized.

After extraction, the DNA associated with the virion and slower migrating particles was examined (Fig. 5C). Single-stranded genomic DNA was associated with the virion peak from the 37°C infection, as was replicative form (RF) DNA, but to a lesser extent. In contrast, RF DNA was predominately associated within the slower particles. Only RF DNA was detected in the lower-temperature samples, indicating that robust packaging only occurred at the higher temperature. The 26°C material contained both supercoiled and relaxed RF DNA, suggesting that protein A's role in nicking RF DNA, a requirement for rolling circle replication, may be less efficient or reflect a more recalcitrant DNA substrate at lower temperatures. The protein and DNA content of the slower migrating particles are consistent with degraded packaging complexes (see Discussion).

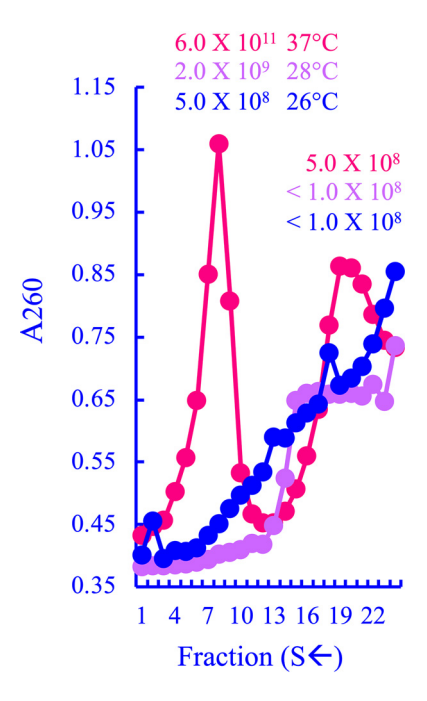


FIG 4 Sedimentation profiles of wild-type $\alpha 3$ infection products generated from 37° (red), 28° (lavender), and 26°C (blue) infections. Material was detected by UV spectroscopy. Lower numbered fractions reflect faster sedimenting material. The titers of the peaks, or regions if a peak was not evident, are given within the figure.

The exogenous expression of cloned A* genes expands the lower-temperature growth limit. Elevated intracellular A* protein levels can rescue \emptyset X174 packaging defects (11). To determine whether they could rescue α 3 low-temperature plaque formation, wild-type α 3 was plated on cells expressing a cloned \emptyset X174 or α 3 A* gene(s). As can be seen in Fig. 3 (blue bar no. 2), cloned \emptyset X174 A* gene expression modestly extended the lower limit. Due to a much larger and clearer plaque morphology, 28°C titers were easily obtained. Unlike \emptyset X174- and G4-like viruses, α 3-like viruses contain at least two A* genes (1), suggesting that these phages may be more dependent on A* function. Indeed, expressing the α 3 A*genes had the most dramatic effect on low-temperature plating efficiency (Fig. 3, blue bars no. 3 and no. 6). Although the plating efficiency was only 10^{-3} at 26° C, it was still 3 orders of magnitude above that of the negative controls (no exogenous A* gene expression and exogenous \emptyset X174 A* gene expression, blue bars no. 4 and no. 5, respectively).

A mutation in the internal scaffolding protein expands the low-temperature growth limit. To determine if the $\alpha 3$ growth range could be expanded in one mutational step, 10^8 to 10^9 phages were plated at 26° C and incubated overnight. No variants were recovered (frequency, $<10^{-8}$), indicating that at least two point mutations are required to overcome low-temperature growth barriers. Elevated A* protein levels appeared to elevate low-temperature plating efficiencies (Fig. 3). Thus, alleviating packaging defects with cloned A* gene expression may facilitate the isolation of low-temperature plaque-forming variants. Due to the higher plaque background associated with cloned $\alpha 3$ A* gene expression, the $\alpha 3$ A* gene expression may facilitate the isolation of low-temperature plaque expression, the $\alpha 3$ A* gene expression, the $\alpha 3$ A* gene expression may facilitate the isolation of low-temperature plaque expression, the $\alpha 3$ A* gene expression may facilitate the isolation of low-temperature plaque expression.

Under these conditions, expanded temperature range variants were recovered at a frequency of 10^{-5} . They were selected from 13 independently generated $\alpha 3$ populations. At least one variant per population was sequenced. All contained a G \rightarrow C transversion at nucleotide 2148. The complete genome of one variant was sequenced. No other mutations were found, indicating that this mutation was both necessary and sufficient for reliable plaque formation growth at 26°C on cells expressing a cloned A* gene. Silent vis-à-vis protein A, the transversion confers a G \rightarrow R substitution at amino acid 118 of the internal scaffolding protein, ltq(B)G118R (low temperature growth

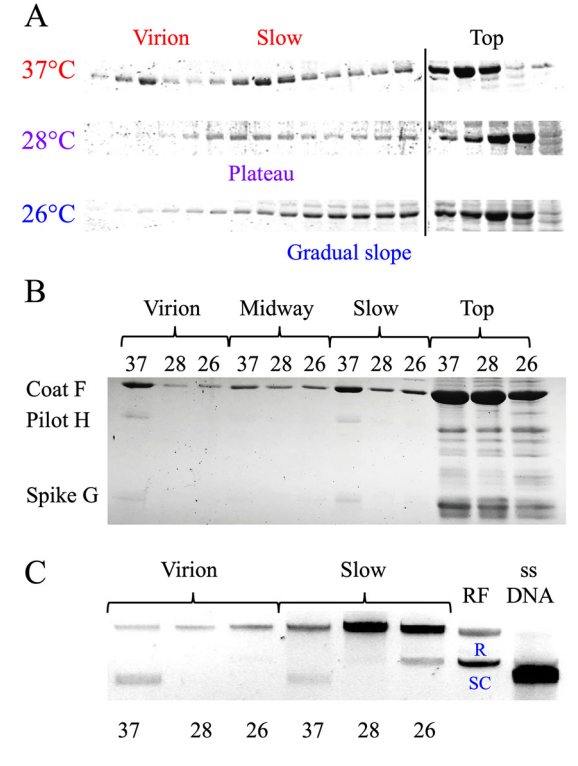


FIG 5 Characterization of fast (virions) and slow migrating particles. (A) The distribution of the coat protein throughout the gradients. Each gradient was separated into ~40 fractions. Every other fraction was analyzed by SDS-PAGE. The position of peaks, plateaus, or slopes from the sedimentation profiles in Fig. 4 are given within the figure. More fractions were analyzed than are depicted within the sedimentation profile. The rightmost five fractions of each gradient were run on a separate gel; hence, the gap within the figure. (B) Side-by-side SDS-PAGE analysis of the fast (virion) and slow sedimenting particles. "Midway" represents material taken from fractions between the two. "Top" indicates the topmost gradient fractions, which would contain material with S values of less than 30. The position of the three major structure proteins is given to the left of the gel. (C) DNA extracted from virions and slow migrating particles. DNA standards are in the rightmost two lanes. Relaxed and supercoiled replicative form (RF) DNA are, respectively, indicated with the letters "R" and "SC."

mutation). As can be seen in Fig. 3 (magenta bars), ltg(B)G118R plates at efficiencies approaching 1.0 at 26°C, regardless of which A* gene was exogenously expressed, plaques were well defined. Without exogenous A* gene expression, plating efficiency falls at least 1 order of magnitude, and the resulting miniscule plaques were difficult to observe.

The mechanism by which the *ltg(B)G118R* mutation rescues, most likely in concert with elevated A* protein levels, is not precisely known. The mutations reside in the C terminus of the protein, which mediates most interactions with the viral coat protein (23–25). It could elevate procapsid formation (Fig. 2); thus, increasing the number of packaging initiation events without altering the probability of a successful outcome. Alternatively, it may affect procapsid stability, which could prevent the formation of off-pathway by-products.

 α 3 can be experimentally evolved to grow at low temperatures. Despite utilizing 13 independent populations in the above-described genetic selections, only one mutation was recovered. Thus, insights were limited. To uncover other mechanisms that may enhance low-temperature growth, the virus was experimentally evolved at successively lower temperatures with and without exogenous A* gene (see Materials and Methods). Briefly, four wild-type and four ltg(B)G118R plaques were isolated at 37°C and placed in 100 μ L of H₂O. The resulting solutions were spotted on lawns containing wild-type cells and cells expressing the cloned α 3 A* gene at 37°C to generate eight control lineages and at a lower temperature to apply selective pressure. For wild-type α 3, the initial low temperature was 28°C, whereas it was 26°C for the ltg(B)G118R

strain. The 37°C plates were incubated for 3 h. Low-temperature plates were incubated for 18 h. Afterward, phages were transferred to freshly seeded plates (see Materials and Methods). This was repeated for 10 cycles. To select for variants that had expanded their low-temperature growth range, approximately 106 PFU from the last cycle were plated at temperatures two degrees lower than the evolution temperature. If a population did not produce a low-temperature variant above a frequency of 10⁻⁴, the lineage was discontinued. If variants were present, the one forming the largest plaque was sequenced and used for the next 10-cycle round of experimental evolution, 2°C lower than the previous one. The 37°C control lineages, eight in total, were continuously transferred at 37°C for 40 cycles. As can be seen in Table 1, plaque-forming variants could be isolated as low as 24°C in wild-type cells, and 22°C with the exogenous expression of the cloned A* gene.

Besides temperature, other factors could influence the spectrum of mutations that arose. This likely included alternating between low-multiplicity of infection (MOI) environments, at the start of incubation, to a high-MOI environment during incubation. In addition, replication would initially occur within exponentially growing cells and later transition to cells either in or approaching the stationary phase. For example, the F-R101 and J-A13S mutations were recovered from both low- and high-temperature passages. Considering that only eight control 37°C lineages were analyzed, this may also apply to other mutations arising only once in the low-temperature lineages. However, several mutations arose independently in multiple lineages and in an apparent temperature-dependent manner.

Genome deletions larger than 200 nucleotides are sufficient to expand the lower-temperature range. All low-temperature lineages acquired a deletion in the H-A intercistronic region, the largest of which was 488 bases. In two lineages, the deletion grew as the incubation temperature was lowered. No deletions developed in the 8 control 37°C lineages. The conserved H-A intercistronic region of the α 3-like viruses is considerably larger than the ones found in sister genera. Apart from the gene A promoter and the gene H transcription terminator (Fig. 1), the function of this large, and clearly unessential, intercistronic region is unknown.

To directly determine the effects of deletions on low-temperature growth, a series of intercistronic deletions were constructed in a wild-type background. Their 5' ends began at nucleotide 95 within the published $\alpha 3$ sequence (6), whereas the 3' ends varied at 100-nucleotide intervals. The resulting mutations were assayed for low-temperature plaque formation and compared to wild-type $\alpha 3$ (Table 2). The ability to form plaques at lower temperature appeared to increase with larger deletions. The strain with the smallest deletion, Δi cr100 (deletion of 100 nucleotides within the intercistronic region), displayed a wild-type phenotype in this assay. Although Δi cr200 could not form plaques on the wild-type host at 26°C, the expression of the exogenous A* genes rescued plaque formation. The effects of the larger deletions (Δi cr300 and Δi cr400) were more pronounced. Neither strain required the exogenous A* gene expression for 26°C plaque formation.

Large deletions can only occur in regions that are not required for viability, such as the H-A intercistronic region. The other intercistronic regions are smaller than 200 nucleotides. Thus, to determine if other deletions in the genome could have a similar effect, a protein-coding sequence would need to be eliminated. Thus, the resulting mutant would require complementation with a cloned essential gene. Two $\alpha 3$ genes are large enough for a 400-base deletion, gene F, which encodes the viral coat protein, and gene H, which encodes the DNA pilot protein. The expression of our cloned $\alpha 3$ F gene proved too toxic for this analysis (26); therefore, a 400-nucleotide deletion was constructed in gene H. The resulting mutant, $\Delta H400$, was assayed for low-temperature plaque formation on cells expressing a cloned $\alpha 3$ H gene. Although no plaque formation was observed at 26°C, it was efficient at 27°C. Plaques were well defined and readily visible. In contrast, wild-type $\alpha 3$ plated poorly under the same conditions; plating efficiency fell at least 1 order of magnitude, and plaques were extremely small, hazy, and ill-defined. These data suggest that genome reduction, in general, may extend the

TABLE 1 The experimental evolution of wild-type α 3 and α 3Ltg(B)

Parent, lineages, and	Next-generation		Plating efficiency ^d A* expression:	
evolution conditions ^a	isolation conditions ^b	Genotype of new isolate ^c	Without Wi	
WT, 28°C	26°C	Δ95-504, A-D55G, J-A13S, F-Y394H	0.8	0.7
WT, 28°C	26°C	Δ90-420, A-Q43R, F-D395G	0.5	0.4
Above isolate, 26°C	24°C	Δ90-420, A-Q43R, F-D395G, A-A417T, B-R68H	$<10^{-3}$	0.05
WT, 28°C	26°C	Δ 102-419, A-E153G & A*re g^e	0.4	1.0
Above isolate, 26°C	24°C	Δ102-419, A-E153G & A*reg, A-T412I, F-L236I	0.03	0.03
WT, 28°C	26°C	Δ61-508, A-E153G and A*reg	0.3	0.7
Above isolate, 26°C	24°C	Δ61-508, A-E153G & A*reg, C3810T (silent)	0.01	0.03
WT, 28°C with A*	26°C with A*	H-K113R	1.0 ^{pp}	1.0
WT, 28°C with A*	26°C with A*	Δ 272-507, A-E153G & A*reg, C3915T (silent)	$< 10^{-2}$	0.3
WT, 28°C with A*	26°C with A*	Δ 96-491, Δ 96-419	1.0	1.0
Above isolate	24°C with A*	Δ 96-491, A-D137G and A*reg, F-A	$<10^{-2}$	0.7
WT, 28°C with A*	26°C with A*	A-K341R	$<10^{-2}$	0.7
Above isolate	24°C with A*	A-K341R, Δ85-508	$< 10^{-2}$	0.7
Ltg(B), 26°C	24°C	B-G118R, Δ 96-419, A-D55G, F-R101C, T4257G (silent), F-Q402H	0.6	1.0
Ltg(B), 26°C	24°C	B-G118R, Δ 96-419, A-D137G and A*reg ^f , F-R101C, F-D393E	0.4	0.9
Ltg(B), 26°C, with A*	24°C, with A*	B-G118R, Δ96-505, A-D137G and A*reg, K-R48H and C-A23T	0.2 ^{pp}	0.5
Above isolate, 24°C, w/A*	22°C, with A*	B-G118R, Δ96-505, A-D137G and A*reg, K-R48H and C-A23T, B-F47L, T6055C (silent)	<10 ⁻³	0.04
Ltg(B), 26°C, with A*	24°C, with A*	B-G118R, Δ96-421, A-D137G and A*reg	0.5 ^{pp}	0.85
Above isolate, 24°C	22°C, with A*	B-G118R, Δ85-573, A-D137G and A*reg, A-S226P, B-R73C, F-V282A	$<10^{-3}$	0.3 ^{pp}
Ltg(B), 26°C, with A*	24°C, with A*	B-G118R, Δ96-470, A-D137G and A*reg	0.3 ^{pp}	1.0
Above isolate, 24°C	22°C, with A*	B-G118R, Δ96-574, A-D137G and A*reg	$< 10^{-3}$	0.1 ^{pp}
		A-K341R, C3810T (silent)		
Ltg(B), 26°C, with A*	24°C, with A*	B-G118R, Δ 96-571, A-D137G and A*reg	0.07 ^{pp}	0.3
Above isolate, 24°C	22°C, with A*	B-G118R, Δ96-571, A-D137G and A*reg D-D38G, F-E145Q, F-V389F	<10 ⁻³	0.05 ^{pr}
WT, 37°C	37°C ^g	C _R -R3W, F-E154G,	NA^h	NA
WT, 37°C	37°C	C _B -R3W	NA^h	NA
WT, 37°C	37°C	C _B reg? ⁱ K-R23G & A-Q489R, F-R101C	NA^h	NA
WT, 37°C	37°C	C _B reg? ⁱ K-R23G & A-Q489R, J-A13S	NA^h	NA
WT, 37°C with A*	37°C	C _B reg? ⁱ K-R23G & A-Q489R	NA^h	NA
WT, 37°C with A*	37°C	C _B -R3W, H-L2F	NA^h	NA
WT, 37°C with A*	37°C	C _B -frameshift [/]	NA^h	NA
WT, 37°C with A*	37°C	C _B -frameshift ⁱ , H-L2F	NA^h	NA
WT, 37°C with A*	37°C	$C_{\rm g}$ -frameshift, $C_{\rm g}$ -L6F	NA^h	NA

The parental strain used in the experiment and the conditions used during its experimental evolution. Dashed lines separate lineages. Thus, entries between lines describe the history of one lineage.

April 2022 Volume 96 Issue 7 10.1128/jvi.01970-21

^bThe conditions utilized to select for a mutant with an expanded low-temperature growth range.

The genotype of the variant that arose. Δ, deletions that occur in a large intercistronic region. The numbers represent the deletion endpoints in the nucleotide sequence. Thus, $\Delta 95-504$ indicates a deletion spanning nucleotides 95 through 504. For mutations that conferred changes in the amino acid sequences, the changes are reported in the following format: Protein, wild-type amino acid, position, new amino acid. Thus, A-D55G represents a D—G change in amino acid 55 of protein A. For mutations that do not alter amino acid sequences, the changes are reported in the following format: wild-type nucleotide, position, new nucleotide, Thus, C3810T represents a C->T transition at nucleotide 3810 in the genome sequence. For structural proteins for which structures have been determined, proteins F and J, the initial methionine is not counted.

^dThe data were normalized to the plating efficiency of the strain under the conditions and temperature at which it was evolved. This value was set to 1.0. The values within the table represent the plating efficiencies determined under the conditions under which the mutant was isolated, which is two degrees lower than the temperature at which it was evolved. Plating efficiency was determined with and without the exogenous expression of the cloned A* gene. pp indicates that plaques were extremely small displaying a faint pin-prick morphology. eThe mutation is 2 nucleotides before the start codon of an A* gene commencing at nucleotide 1170.

The mutation is in an A* start RBS for the A* gene commencing with nucleotide 1221 and 2 nucleotides after the A* gene beginning with nucleotide 1212.

 $^{{}^}g$ Wild-type lineages generated at 37C were continually passaged for 40 passes. Each entry represents a distinct lineage.

^hThe control lineages did not expand their lower-temperature growth range.

The nucleotide substitution is three nucleotides upstream from the C_B gene RBS. Its effects on CB gene translation have not been directly tested.

The C_B frameshifts were not identical.

TABLE 2 Low-temperature plating efficiency of α 3 mutants with deletions in the H-A intercistronic region normalized to 37°C data

	Exogenous gene expression:		
Strain	None 26°C	α3A* 26°C	
Wild type	<10 ⁻⁵	<10 ⁻⁵	
Δicr100	<10 ⁻⁴	<10 ⁻⁴	
Δicr200	<10 ⁻⁴	0.2	
Δ icr300	0.1	0.7	
Δ icr400	0.3	0.9	
	Cloned H gene expression	:	
	26°C	27°C	
Wild type	<10 ⁻⁵	10^{-1} – 10^{-2a}	
ΔH400	<10 ⁻⁵	1.0	

^aPlating efficiency was approximated for this condition. Plaques displayed a faint pin-prick morphology, which hindered accurate counts.

lower range of plaque formation. Beyond this conclusion, insights are limited. Strains with deleted coding sequences must be complemented. Thus, results could be influenced by complementation efficiency and the general effects of cloned phage gene expression on host cell physiology. Thus, any additional advantage that a specific deletion may confer cannot be determined.

Adaptation alters A* gene expression on the translational level. Either one of two mutations (A1217G and A1168G) arose independently in 75% of the low-temperature lineages but were not found in the eight 37°C control lineages. Although these substitutions change the primary structure of protein A, they are also very near gene A* start codons, suggesting a possible effect on gene expression. It is also 2 bases after the end of the A* start codon spanning nucleotides 1212 to 1215 (Fig. 6A). Similarly, the A1168G mutation is 2 nucleotides before a possible A* start codon at nucleotide 1170.

Microvirus gene expression is primarily controlled by *cis*-acting genetic elements (27), which are canonical in nature. However, poorly understood noncanonical mechanisms have been noted (22, 28, 29). Indeed, a recently determined high-resolution ØX174 transcription map documented several previously unknown and poorly understood regulatory mechanisms (29). Consequently, the effects that the 1168 and 1217 mutations may have on protein A* translation cannot be predicted. Therefore, a series of reporter genes were constructed using pLES94 (30), a promoterless plasmid containing a *lacZ* gene.

Gene A* transcripts are produced from the P_A promoter, the weakest of the well-characterized promoters (29), which produces unstable transcripts (29, 31). To ensure that the surrogate system resembled the biological context in which gene A* would be expressed, the entire sequence between the P_A promoter and the A* start codons was cloned into the vector (Fig. 6A). A wild-type (WT) and a mutant (MUT) version were constructed for each plasmid. The vectors were placed into a Lac⁻ cell line (Top10; Invitrogen), and betagalactosidase activity was determined. The negative control contained a promoterless vector, whereas the positive standard was an induced Lac⁺ *E. coli* strain (C122).

Figure 6B displays the results obtained from two biological replicates of each reporter gene. Each biological replicate incorporated three technical replicates. The activity associated with the wild-type fusions (WT1168 and WT1217) were modest compared to the positive standard (Lac⁺ in the figure) but 2 orders of magnitude above the negative empty vector (EV) control. For graphing the data on a log scale, the activity associated with the negative standard (EV) was set at 0.1. The actual values were below 0. The mutations at 1168 and 1217 (MUT1168 and MUT1217) elevated Miller units over those obtained from their respective wild-type recorder genes (WT1168 and WT1217). The elevated levels were statistically significant (P < 0.0001). The effects of the 1217 mutation were particularly pronounced. This mutation resides between two A* start codons. However, it is unclear which one, or both, is affected by the mutation.

Other mutations that arose during low-temperature adaptation. Numerous other mutations arose during the low-temperature adaptation. Unlike the deletions

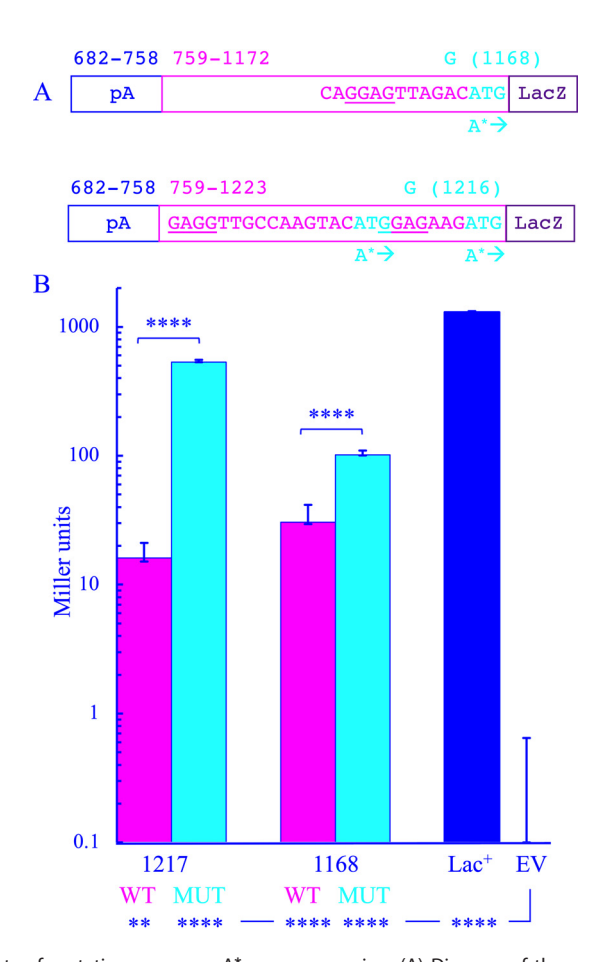


FIG 6 The effects of mutations on gene A* gene expression. (A) Diagram of the reporter genes used in these studies. Numbers refer to the $\alpha 3$ nucleotide sequence (6) inserted into pLES94 (30). A* start codons are highlighted in cyan. The nucleotide substitutions found in the evolved strains are depicted in cyan above the map. Ribosome binding sites are underlined. (B) Miller units generated by the reporter genes. The numbers 1217 and 1168 refer to the location of the nucleotide substitutions within the $\alpha 3$ gene sequence. WT (wild-type) and MUT (mutant) indicate whether the reporter construct contains the mutation found in the evolved $\alpha 3$ strains. Lac+ refers to an induced culture of wild-type *E. coli* C122. EV refers to the lac- strain carrying an empty pLES94 vector. The graph depicts data generated from two biological replicates, each one incorporating three technical replicates. The values obtained from the biological replicates were statistically indistinguishable. Therefore, the data sets were combined. Thus, columns and standard deviations in Fig. 5B incorporate six data points. Statistical analysis was performed by one-way ANOVA with Tukey's multiple-comparison test (**, P < 0.001; *****, P < 0.0001). P values for comparisons with the EV sample are given below the x axis, whereas P values for comparisons between respective WT and MUT reporter genes are contained within the figure.

and the mutations involved in A* gene expression, these appeared in only one or two lineages. These may reflect a more subtle mechanism to increase low-temperature fitness and are distinct from DNA synthesis and packaging (see Discussion).

Adaptation at 37°C altered DNA metabolism but in a fundamentally different manner. As a control for low-temperature lineages, wild-type $\alpha 3$ was passaged 40 times on plates at 37°C. Eight lineages were generated, four with and four without exogenous A* gene expression (Table 1). At least six of the eight lineages contained a mutation that likely affects C_B gene expression. Unlike the sister genus viruses, $\alpha 3$ -like phages contain two C genes (7). The larger version, C_B , is translated from a GTG start codon upstream from the ATG start codon of the smaller version, C_S (Fig. 1). Both genes have easily discerned ribosome binding sites (RBS). In some lineages, the C_B proteins would be eliminated via frameshift mutations, which affect neither the coding sequence nor the RBS of the downstream C_S gene. Frameshifts in the C_B gene confer resistance to the inhibitory effects conferred by the overexpression of the host cell ssb gene (7) and can affect the timing of ssDNA gene expression (see Discussion).

DISCUSSION

DNA packaging constrains α **3 virion production at low temperature.** Below 28°C, virion production was dramatically lower than that of the 37°C permissive infection. However, noninfectious slower migrating particles accumulated. Similar particles were detected at 37°C but did not predominate over virions. These particles contain assembled coat protein and RF DNA. In the 37°C samples, which had the highest optical density, the spike G and DNA pilot H proteins were also detected. The external scaffolding protein, the most abundant procapsid component, was notably absent. ØX174 procapsids are known to lose their external scaffolding protein during sample preparation (17, 19–22), producing empty capsids, which migrate more slowly than virions. However, RF DNA is not typically associated with ØX174 degraded procapsids. Thus, the protein and DNA content of the slower migrating α 3 particles are consistent with degraded or off-pathway packaging complexes (32, 33).

Low-temperature adaptation modified the packaging substrate. To overcome inhibitions to low temperature packaging, genome deletions accrued within the packaging substrates. DNA persistence lengths, a measure of polymer flexibility, inversely increase as a function of temperature (15). Thus, smaller genomes may compensate for more rigid DNA substrates. All deletions occurred within an unessential portion of the very large H-A intercistronic region, which is the only region large enough to tolerate them. The other intercistronic regions are considerably smaller and contain regulatory elements.

To determine whether other large deletions could have a similar effect, 400 nucleotides were removed from gene H, which could be complemented by a cloned H gene. Although the resulting strain plated more efficiently than the wild type at lower temperatures, rescue was not as robust as those observed with the intercistronic deletions. This could reflect an allele-specific advantage of H-A intercistronic deletions. The potential gene products produced by the small ORFs found in the intercistronic region may actively inhibit low-temperature growth. Alternatively, and equally likely, the less robust rescue by the gene H deletion could be the consequence of using a complementation-dependent strain.

The genetically engineered H-A intercistronic deletion mutants did display modestly smaller plaque morphologies at 42°C. This may reflect a possible function for the potential ORF gene products, which are conserved throughout the α 3 genera, but does not exclude other explanations, such as unforeseen effects on gene regulation. This region's contribution to fitness may also be partly physical or structural. The α 3 capsid may require a larger genome for optimal fitness for reasons other than coding capacity (34, 35). Thus, any conclusions regarding functions associated with this intercistronic region would be highly speculative.

Low-temperature adaptation modified the packaging reaction. Genome biosynthesis and packaging are concurrent processes. As the daughter (+) strand is synthesized, the parental (+) strand is displaced and guided into the capsid via its interactions with J and viral coat proteins. Thus, the rate of strand displacement versus ssDNA synthesis may be important. If synthesis outpaces displacement, unpackaged, ssDNA could accumulate and lead particles off-pathway. Protein A* binds to at least 30 degenerate sequences throughout the genome (36). Once attached, it inhibits the unwinding of the dsDNA template. (37), slowing replication. Indeed, elevated A* protein levels rescue packaging defects that prevent filling capsids to completion (11) but does not rescue defects that produce fully filled particles that lack infectivity (19). Even in the absence of other mutations, the exogenous expression of cloned A* genes extended the lower range of wild-type $\alpha 3$ growth, albeit modestly. The relative increase in intracellular A* protein concentration resulting from cloned gene expression is unknown and cannot easily be predicted. First, gene expression is induced by arabinose, which will be catabolized. Thus, there will be kinetic effects (38). Second, the arabinose promoter is strongly regulated by catabolite repression, as is the expression of other alternate carbon source catabolic pathways that would be active when cells are grown in media containing tryptone and yeast extract (38). However, expression is likely low. Exogenous A* gene

expression is extremely toxic to cells when expressed from strong promoters (39). Regardless of the level of cloned A* gene expression, Viral A* gene expression was critical to extending the low-temperature growth range. During adaptation, mutations that affect genomic A* gene regulation were the second most common, affecting 3/4 of the low-temperature lineages. These mutations were not observed in any of the 37°C control lineages. Clustering in or adjacent to A* ribosome binding sites, they dramatically increased A* protein translation within the context of the recorder gene assay.

Mutations that may alter the timing of DNA packaging arose at elevated **temperatures.** As a control for the low-temperature lineages, wild-type $\alpha 3$ was continually passaged at 37°C, and all lineages acquired mutations in the C_B gene that did affect the coding sequence of the smaller C_s gene. In many cases, these mutations produced frameshifts that would prevent C_B protein production. The elimination of the C_B protein most likely affects the switch from dsDNA (stage II) synthesis to ssDNA (stage III) synthesis. Both in vivo and in vitro, C proteins compete with the host cell SSB protein for binding the origin of replication (7, 8). If bound by SSB, another round of stage II DNA synthesis occurs. If bound by protein C, single-stranded genomes are synthesized packaging. The overexpression of the host ssb gene significantly inhibits α 3 replication. Frameshifts in the C_B gene, as seen in this current study, restore viability (7). Thus, at 37°, it may be advantageous to produce progeny more quickly by expediting the switch to ssDNA replication. The molecular basis of this competition is likely more complicated during an α 3 infection, which produces a version of the C protein, than during an \emptyset X174 infection. C protein acts as a dimer (40). Therefore, three types of α 3 C protein dimers can theoretically be produced— $C_BC_{B'}$, $C_BC_{S'}$ and C_SC_S . The elimination of the C_B isoform suggests the C_sC_s dimers, the one dimer produced in some of the 37°C evolved lineages, more effectively competes with SSB. Although this interpretation is consistent with the phenomenon described here and previously reported (7), it has yet to be tested in

Other inefficient functions at low temperature. Vis-à-vis its ability to replicate at low temperatures, the evolutionary history of $\alpha 3$ is unknown. Whether its ancestor lost the ability to grow at low temperatures or never evolved this capability cannot be determined. As genome size precludes low-temperature virion production, it is likely that other functions may operate less efficiently, which could further prevent replication. However, the data set presented here lacks the depth to identify these functions. Unlike the deletions and the mutations affecting A* protein synthesis, most mutations only arose in one or two lineages. However, the coat protein mutations located between residues 389 and 402 and at 364, fall within a region for which published experimental data exist (26). In the atomic structure of the α 3 virion (16), these residues reside in the coat-spike protein interface (Fig. 7). This interface acts as the antireceptor for the host cell lipopolysaccharide, which triggers the removal of the spike protein pentamer at the vertex in contact with the cell surface (41). Mutations within the region, in particular residues 393 to 402, are known to expand the host range of wildtype α 3 (26). Thus, these substitutions could facilitate host cell interactions at lower temperatures. Alternatively, they may stabilize coat-spike protein interactions during assembly or within the virion.

MATERIALS AND METHODS

Phage plating, media, buffers, stock preparation, and bacterial and phage strains. The plating protocol, media, buffers, stock preparation, and wild-type *Escherichia coli* C122 strain have been previously described (42). The RY7211 cell line contains a mutation in the mraY gene, conferring resistance to viral E protein-mediated lysis (43). Bacteriophage α 3 was originally isolated in the early 1960s (44), a labadapted strain (6) was sequenced in 1992 (GenBank accession no. X60322.1), which was 6,087 nucleotides in length. A new isolate was sequenced in 2006 (GenBank accession no. DQ085810.2), which contained 6,089 nucleotides (1). The 2006 sequence was the reference sequence used in these studies. The nucleotide changes found in our strain of α 3 and the mutants isolated in this study can be found in Table S1 in the supplemental material.

Gene cloning. The cloning of the α 3 H gene (26) and the ØX174 A* gene (11) have been previously described. Like the ØX174 A* gene, the α 3 A* genes were cloned into pBAD33 (38). The A* genes, residing between nucleotides 1158 and 2159, along with the ribosome binding site of the longest gene,

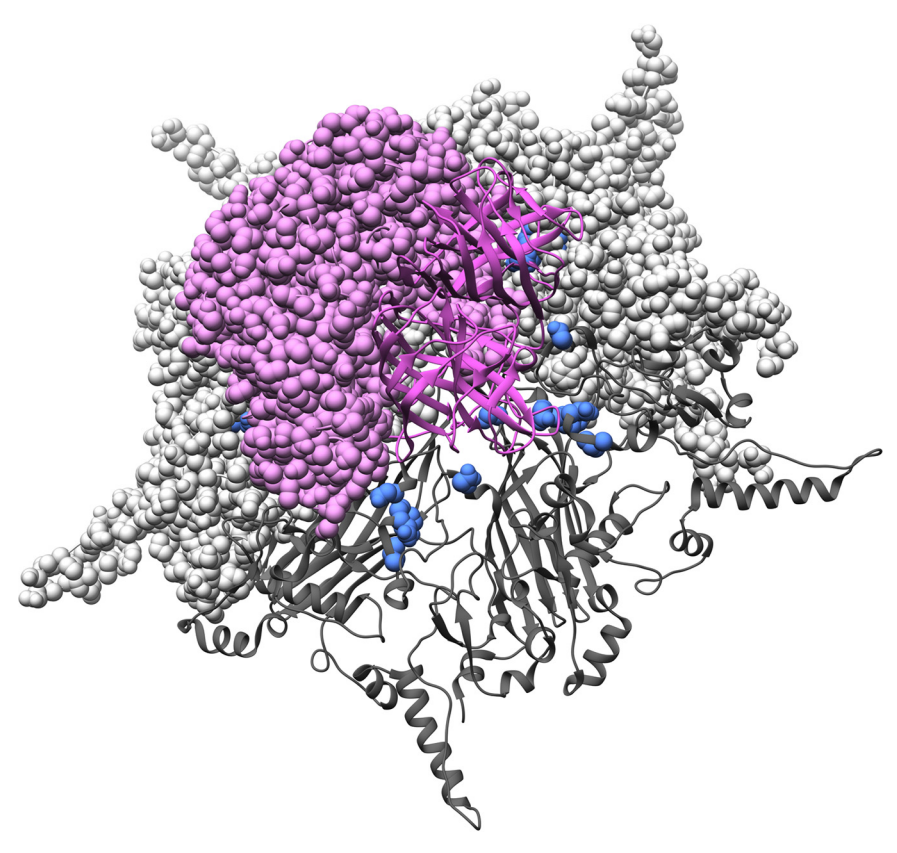


FIG 7 Coat protein mutations residing within the coat-spike protein interface. The coat and spike proteins are depicted in magenta and gray, respectively. The locations of the substitutions found in the low-temperature-adapted strains are depicted in light blue. The image was generated using Chimera (48) and Protein Data Bank accession code 1M06.

were PCR amplified with primers that introduced upstream Xbal and downstream HindIII sites. The template DNA contained an amber mutation in the overlapping B gene. The resulting fragment was digested with Xbal and HindIII and ligated into pBAD33 (Thermo Fisher) treated with the same enzymes. Gene expression was induced by supplementing media with 0.2% arabinose and repressed with 0.2% glucose.

Experimental evolution. Four wild-type and four Itg(B)G118R plaques were isolated at 37°C and placed into 100 μ L of H₂O. Then, 5.0 μ L of each solution was spotted on 4 lawns: (i) wild-type cells incubated at 37°C, (ii) cells expressing the cloned α 3 A* gene incubated at 37°C, (iii) wild-type cells incubated at 28°C, for wild-type α 3, or 26°C for Itg(B)G118R, and (iv) cells expressing the cloned α 3 A* gene incubated at 28°C (wild-type α 3) or 26°C [Itg(B)G118R]. The 37°C plates were incubated for 3 h. Low-temperature plates were incubated for 18 h. After incubation, each clearing was stabbed multiple times with a toothpick to transfer phage to freshly seeded plates. After this process was repeated for 10 cycles, phages were collected from each clearing to generate solutions approximating 10° PFU/mL. To select for variants with an expanded low-temperature growth range, the population was plated 2°C lower than the evolution temperature. If a plaque could not be obtained above a frequency of 10⁻⁴, compared to the titer at the evolution temperature, the lineage was discontinued. If plaques formed, the largest one was placed in 100 μ L H₂O. The genome was sequenced, and the solution was used to conduct the next 10-cycle round of evolution, 2°C lower than the previous 10 cycles. The 37°C control lineages, eight in total, were continuously transferred at 37°C for 40 cycles.

Construction of $\alpha 3$ strains with deletions in the H-A intercistronic region and in gene H. Strains with deletions in the H-A intercistronic region were generated by PCR using the high-fidelity Q5 DNA polymerase (New England Biolabs). Apart from the region to be deleted, the entire genome was amplified to produce a linear PCR product. The 5' end of all deletions began at nucleotide 95, whereas the 3' ends were progressively increased in increments of 100 nucleotides. The 5' hydroxyl termini were phosphorylated using T4 polynucleotide kinase, and the ends were joined using T4 DNA ligase (New England Biolabs). Deletion mutants were recovered in wild-type cells at 37°C. The H gene deletion spans nucleotide 5176 to 5588 and was constructed in a similar manner but recovered in cells expressing a cloned $\alpha 3$ H gene (26).

Reporter gene construction and assays. To construct the A* reporter genes, wild-type α 3 DNA was PCR amplified starting at nucleotide 684, to include promoter from which A* genes are transcribed and ending at the A* gene start codons at nucleotide 1168 or 1216. The upstream primer contained a HindIII

site at the 5' end, whereas the downstream primers contained a BamHl site. The resulting fragments were digested with HindIII and BamHl and ligated into pLES94 (30) treated with the same enzymes. Thus, the clones contained the α 3 regulatory regions fused to a *lacZ* gene. The plasmids were transformed into *E. coli* Top10 cells (Invitrogen), genotype F-mcrA Δ (mrr-hsdRMS-mcrBC) φ 80lacZ Δ M15 Δ lacX74 recA1 araD139 Δ (ara-leu)7697 galU galK rpsL (StrR) endA1 nupG.

Reporter gene assays were conducted as previously described (45) with minor modifications. Briefly, cells were grown to concentrations of $\sim\!3.0\times10^8$ cells mL. Then, 1.0 mL was concentrated by centrifugation, and the cell pellet was resuspended in 2.0 mL of chilled Z buffer (60 mM Na_2HPO4, 40 mM NaH_2PO4, 10 mM KCl, 1.0 mM MgSO4, 50 mM β -mercaptoethanol, [pH 7.00]). To permeabilize the cells, 0.1 mL of CHCl3 and 0.05 mL of a sodium dodecyl sulfate solution (0.1% wt/vol) were added. Samples were incubated for 5.0 min at 28°C before the addition of 0.2 mL of an ortho-nitrophenyl- β -galactoside solution (4.0 mg/mL in 60 mM Na_2HPO4, 40 mM NaH_2PO4 [pH 7.0]). Reaction mixtures were incubated for 27 min before the addition of 0.5 mL of 1 M Na_2CO3, which stopped the reactions. The absorbance at 420 nm and 550 nm was measured for each sample, and Miller units were calculated as previously described (45). Statistical analysis was conducted using GraphPad Prism version 9. One-way analysis of variance (ANOVA) with Tukey's multiple-comparison tests was performed on aggregate values from two biological replicates performed in technical triplicate. An adjusted P value of <0.01 was considered significant.

Infected cell extracts and rate zonal sedimentation. To characterize infection products, infected cell extracts were prepared from 100 mL of lysis-resistant cells (1.0 \times 108 cells/mL) infected at a multiplicity of infection (MOI) of 3.0. The 37°C infections were incubated for 3 h, whereas the 28°C and 26°C infections were incubated for 6 h. Infected cells were concentrated and resuspended in 2.0 mL sucrose gradient buffer (SGB; 100 mM NaCl, 5.0 mM EDTA [ethylenediaminetetraacetic acid], 6.4 mM Na₂HPO₄, 3.3 mM KH₂PO₄ [pH 7.0]) and then lysed by an overnight incubation with lysozyme (2.0 mg/mL). After removing cellular debris, the supernatants were concentrated to 200 μ L in a Corning Spin-X spin column (100 kDa cutoff) and loaded atop a 5.0 mL, 5 to 30% (wt/vol) sucrose gradient. Gradients were spun at 192,000 \times g for 1 h and then separated into 125- μ L fractions. Assembled particles were detect by UV spectroscopy (A₂₆₀ and A₂₆₀).

Single-stranded DNA (ssDNA), replicative-form (RF) double-stranded DNA (dsDNA), assembled particle-associated DNA purification, and extracts for sucrose gradient sedimentation. ssDNA was generated and purified with the OLT (Our Little Trick) protocol, which has been previously described in detail (46), as has the protocol used for RF dsDNA purification (47). To isolate DNA associated with assembled particles, 500 μ L of gradient fractions were diluted 2-fold in 10 mM Tris-HCl (pH 7.5)/10 mM NaCl/1.0 mM EDTA. Sodium dodecyl sulfate (SDS), pronase, and additional EDTA were added to respective final concentrations of 0.5% (wt/vol), 0.5 mg/mL, and 10 mM. Samples were incubated at 37°C for 2.5 h before DNA was extracted as previously described (11).

SUPPLEMENTAL MATERIAL

Supplemental material is available online only. **SUPPLEMENTAL FILE 1**, XLSX file, 0.01 MB.

ACKNOWLEDGMENTS

This research was supported by National Science Foundation grants MCB 2013653 (B.A.F.) and U.S. Department of Agriculture Hatch funds to the University of Arizona. We thank M. Rendon and M So for the lavish gift of pLES94.

REFERENCES

- 1. Rokyta DR, Burch CL, Caudle SB, Wichman HA. 2006. Horizontal gene transfer and the evolution of microvirid coliphage genomes. J Bacteriol 188:1134–1142. https://doi.org/10.1128/JB.188.3.1134-1142.2006.
- Hayashi MN, Hayashi M. 1981. Stability of bacteriophage phi X174-specific mRNA in vivo. J Virol 37:506–510. https://doi.org/10.1128/JVI.37.1.506-510 .1981.
- Williams RC, Fisher HW. 1980. Electron microscopic determination of the preferential binding sites of Escherichia coli RNA polymerase to phi X174 replicative form DNA. J Mol Biol 140:435–439. https://doi.org/10.1016/ 0022-2836(80)90393-9.
- Sanger F, Coulson AR, Friedmann T, Air GM, Barrell BG, Brown NL, Fiddes JC, Hutchison CA, Ill, Slocombe PM, Smith M. 1978. The nucleotide sequence of bacteriophage phiX174. J Mol Biol 125:225–246. https://doi.org/10.1016/ 0022-2836(78)90346-7.
- Godson GN, Barrell BG, Staden R, Fiddes JC. 1978. Nucleotide sequence of bacteriophage G4 DNA. Nature 276:236–247. https://doi.org/10.1038/ 276236a0.
- Kodaira K, Nakano K, Okada S, Taketo A. 1992. Nucleotide sequence of the genome of the bacteriophage alpha 3: interrelationship of the genome structure and the gene products with those of the phages, phi X174, G4

- and phi K. Biochim Biophys Acta 1130:277–288. https://doi.org/10.1016/0167-4781(92)90440-B.
- 7. Doore SM, Baird CD, Roznowski AP, Fane BA, 2012 University of Arizona Virology Undergraduate Lab. 2014. The evolution of genes within genes and the control of DNA replication in microviruses. Mol Biol Evol 31: 1421–1431. https://doi.org/10.1093/molbey/msu089.
- Aoyama A, Hayashi M. 1986. Synthesis of bacteriophage phi X174 in vitro: mechanism of switch from DNA replication to DNA packaging. Cell 47: 99–106. https://doi.org/10.1016/0092-8674(86)90370-3.
- 9. Linney E, Hayashi M. 1973. Two proteins of gene A of psiX174. Nat New Biol 245:6–8. https://doi.org/10.1038/newbio245006a0.
- 10. Kornberg A. 1980. DNA replication. Freeman, San Francisco, CA.
- Roznowski AP, Doore SM, Kemp SZ, Fane BA. 2020. Finally, a role befitting Astar: strongly conserved, unessential microvirus A* proteins ensure the product fidelity of packaging reactions. J Virol 94:e01593-19. https://doi .org/10.1128/JVI.01593-19.
- Chejanovsky N, Carter BJ. 1989. Mutagenesis of an AUG codon in the adeno-associated virus rep gene: effects on viral DNA replication. Virology 173:120–128. https://doi.org/10.1016/0042-6822(89)90227-4.

April 2022 Volume 96 | Issue 7 10.1128/jvi.01970-21

- Mankertz A, Hillenbrand B. 2001. Replication of porcine circovirus type 1 requires two proteins encoded by the viral rep gene. Virology 279: 429–438. https://doi.org/10.1006/viro.2000.0730.
- Bowes JM, Dowell CE. 1974. Purification and some properties of bacteriophage ST-1. J Virol 13:53–61. https://doi.org/10.1128/JVI.13.1.53-61.1974.
- Geggier S, Kotlyar A, Vologodskii A. 2011. Temperature dependence of DNA persistence length. Nucleic Acids Res 39:1419–1426. https://doi.org/ 10.1093/nar/qkg932.
- Bernal RA, Hafenstein S, Olson NH, Bowman VD, Chipman PR, Baker TS, Fane BA, Rossmann MG. 2003. Structural studies of bacteriophage alpha3 assembly. J Mol Biol 325:11–24. https://doi.org/10.1016/s0022-2836(02)01201-9.
- McKenna R, Bowman BR, Ilag LL, Rossmann MG, Fane BA. 1996. Atomic structure of the degraded procapsid particle of the bacteriophage G4: induced structural changes in the presence of calcium ions and functional implications. J Mol Biol 256:736–750. https://doi.org/10.1006/jmbi.1996.0121.
- McKenna R, Xia D, Willingmann P, Ilag LL, Krishnaswamy S, Rossmann MG, Olson NH, Baker TS, Incardona NL. 1992. Atomic structure of singlestranded DNA bacteriophage phi X174 and its functional implications. Nature 355:137–143. https://doi.org/10.1038/355137a0.
- Ogunbunmi ET, Roznowski AP, Fane BA. 2021. The effects of packaged, but misguided, single-stranded DNA genomes are transmitted to the outer surface of the oX174 capsid. J Virol 95:e0088321. https://doi.org/10 .1128/JVI.00883-21.
- Uchiyama A, Chen M, Fane BA. 2007. Characterization and function of putative substrate specificity domain in microvirus external scaffolding proteins. J Virol 81:8587–8592. https://doi.org/10.1128/JVI.00301-07.
- Uchiyama A, Fane BA. 2005. Identification of an interacting coat-external scaffolding protein domain required for both the initiation of phiX174 procapsid morphogenesis and the completion of DNA packaging. J Virol 79:6751–6756. https://doi.org/10.1128/JVI.79.11.6751-6756.2005.
- Uchiyama A, Heiman P, Fane BA. 2009. N-terminal deletions of the phiX174 external scaffolding protein affect the timing and fidelity of assembly. Virology 386:303–309. https://doi.org/10.1016/j.virol.2009.01.030.
- Gordon EB, Knuff CJ, Fane BA. 2012. Conformational switch-defective øX174 internal scaffolding proteins kinetically trap assembly intermediates before procapsid formation. J Virol 86:9911–9918. https://doi.org/10 1128/IVI 01120-12
- Dokland T, Bernal RA, Burch A, Pletnev S, Fane BA, Rossmann MG. 1999.
 The role of scaffolding proteins in the assembly of the small, single-stranded DNA virus phiX174. J Mol Biol 288:595–608. https://doi.org/10.1006/jmbi.1999.2699.
- Dokland T, McKenna R, Ilag LL, Bowman BR, Incardona NL, Fane BA, Rossmann MG. 1997. Structure of a viral procapsid with molecular scaffolding. Nature 389:308–313. https://doi.org/10.1038/38537.
- Roznowski AP, Young RJ, Love SD, Andromita AA, Guzman VA, Wilch MH, Block A, McGill A, Lavelle M, Romanova A, Sekiguchi A, Wang M, Burch AD, Fane BA. 2019. Recessive host range mutants and unsusceptible cells that inactivate virions without genome penetration: ecological and technical implications. J Virol 93:e01767-18. https://doi.org/10.1128/JVI.01767-18.
- 27. Hayashi M, Aoyama A, Richardson DL, Hayashi NM. 1988. Biology of the bacteriophage øX174, p 1–71. *In* Calendar R (ed), The bacteriophages, vol 2. Plenum Press, New York, NY.
- Doore SM, Fane BA. 2015. The kinetic and thermodynamic aftermath of horizontal gene transfer governs evolutionary recovery. Mol Biol Evol 32: 2571–2584. https://doi.org/10.1093/molbev/msv130.
- Logel DY, Jaschke PR. 2020. A high-resolution map of bacteriophage varphiX174 transcription. Virology 547:47–56. https://doi.org/10.1016/j.virol .2020.05.008.
- Silver LE, Clark VL. 1995. Construction of a translational lacZ fusion system to study gene regulation in Neisseria gonorrhoeae. Gene 166:101–104. https://doi.org/10.1016/0378-1119(95)00605-6.

- 31. Hayashi M, Fujimura FK, Hayashi M. 1976. Mapping of in vivo messenger RNAs for bacteriophage phiX-174. Proc Natl Acad Sci U S A 73:3519–3523. https://doi.org/10.1073/pnas.73.10.3519.
- Ekechukwu MC, Oberste DJ, Fane BA. 1995. Host and phi X 174 mutations affecting the morphogenesis or stabilization of the 50S complex, a singlestranded DNA synthesizing intermediate. Genetics 140:1167–1174. https:// doi.org/10.1093/genetics/140.4.1167.
- Fujisawa H, Hayashi M. 1976. Viral DNA-synthesizing intermediate complex isolated during assembly of bacteriophage phi X174. J Virol 19: 409–415. https://doi.org/10.1128/JVI.19.2.409-415.1976.
- 34. Chechetkin VR, Lobzin VV. 2017. Large-scale chromosome folding versus genomic DNA sequences: a discrete double Fourier transform technique. J Theor Biol 426:162–179. https://doi.org/10.1016/j.jtbi.2017.05.033.
- Chechetkin VR, Lobzin VV. 2018. Genome packaging within icosahedral capsids and large-scale segmentation in viral genomic sequences. J Biomol Struct Dyn 37:2322–2338. https://doi.org/10.1080/07391102.2018.1479660.
- Langeveld SA, van Mansfeld AD, van der Ende A, van de Pol JH, van Arkel GA, Weisbeek PJ. 1981. The nuclease specificity of the bacteriophage phi X174 A* protein. Nucleic Acids Res 9:545–562. https://doi.org/10.1093/nar/9.3.545.
- Eisenberg S, Ascarelli R. 1981. The A* protein of phi X174 is an inhibitor of DNA replication. Nucleic Acids Res 9:1991–2002. https://doi.org/10.1093/ nar/9.8.1991.
- Guzman LM, Belin D, Carson MJ, Beckwith J. 1995. Tight regulation, modulation, and high-level expression by vectors containing the arabinose PBAD promoter. J Bacteriol 177:4121–4130. https://doi.org/10.1128/jb.177.14.4121-4130.1995.
- Colasanti J, Denhardt DT. 1985. Expression of the cloned bacteriophage phi X174 A* gene in Escherichia coli inhibits DNA replication and cell division. J Virol 53:807–813. https://doi.org/10.1128/JVI.53.3.807-813.1985.
- Aoyama A, Hamatake RK, Mukai R, Hayashi M. 1983. Purification of phi X174 gene C protein. J Biol Chem 258:5798–5803. https://doi.org/10.1016/S0021 -9258(20)81964-4.
- 41. Sun Y, Roznowski AP, Tokuda JM, Klose T, Mauney A, Pollack L, Fane BA, Rossmann MG. 2017. Structural changes of tailless bacteriophage PhiX174 during penetration of bacterial cell walls. Proc Natl Acad Sci U S A 114:13708–13713. https://doi.org/10.1073/pnas.1716614114.
- 42. Fane BA, Hayashi M. 1991. Second-site suppressors of a cold-sensitive prohead accessory protein of bacteriophage phi X174. Genetics 128: 663–671. https://doi.org/10.1093/genetics/128.4.663.
- Bernhardt TG, Struck DK, Young R. 2001. The lysis protein E of phi X174 is a specific inhibitor of the MraY-catalyzed step in peptidoglycan synthesis. J Biol Chem 276:6093–6097. https://doi.org/10.1074/jbc.M007638200.
- 44. Bradley DE. 1963. The structure of coliphages. J Gen Microbiol 31:435–445. https://doi.org/10.1099/00221287-31-3-435.
- 45. Miller JH. 1972. Experiments in molecular genetics. Cold Spring Harbor Laboratory, Cold Spring Harbor, NY.
- Blackburn BJ, Li S, Roznowski AP, Perez AR, Villarreal RH, Johnson CJ, Hardy M, Tuckerman EC, Burch AD, Fane BA. 2017. Coat protein mutations that alter the flux of morphogenetic intermediates through the phiX174 early assembly pathway. J Virol 91:e01384-17. https://doi.org/10.1128/JVI .01384-17.
- Burch AD, Ta J, Fane BA. 1999. Cross-functional analysis of the Microviridae internal scaffolding protein. J Mol Biol 286:95–104. https://doi.org/10.1006/imbi.1998.2450.
- 48. Pettersen EF, Goddard TD, Huang CC, Couch GS, Greenblatt DM, Meng EC, Ferrin TE. 2004. UCSF Chimera: a visualization system for exploratory research and analysis. J Comput Chem 25:1605–1612. https://doi.org/10.1002/jcc.20084.